

Hindered alignment in ultrashort, intense laser-induced fragmentation of O₂

Cite as: J. Chem. Phys. **152**, 014302 (2020); <https://doi.org/10.1063/1.5130706>

Submitted: 07 October 2019 . Accepted: 12 December 2019 . Published Online: 02 January 2020

Arnab Sen, T. Sairam, S. R. Sahu , Bhas Bapat , R. Gopal , and V. Sharma 



View Online



Export Citation



CrossMark

ARTICLES YOU MAY BE INTERESTED IN

Femtochemistry under scrutiny: Clocking state-resolved channels in the photodissociation of CH₃I in the A-band

The Journal of Chemical Physics **152**, 014304 (2020); <https://doi.org/10.1063/1.5134473>

Quantum control of radical pair reactions by local optimization theory

The Journal of Chemical Physics **152**, 014301 (2020); <https://doi.org/10.1063/1.5131557>

Photodissociation of HCl in the photon energy range 14.6–15.0 eV: Channel-resolved branching ratios and fragment angular distributions

The Journal of Chemical Physics **152**, 014309 (2020); <https://doi.org/10.1063/1.5140614>

Lock-in Amplifiers

Find out more today



Zurich
Instruments



Hindered alignment in ultrashort, intense laser-induced fragmentation of O₂

Cite as: J. Chem. Phys. 152, 014302 (2020); doi: 10.1063/1.5130706

Submitted: 7 October 2019 • Accepted: 12 December 2019 •

Published Online: 2 January 2020



View Online



Export Citation



CrossMark

Arnab Sen,¹ T. Sairam,² S. R. Sahu,³  Bhas Bapat,¹  R. Gopal,^{2,a)}  and V. Sharma^{3,b)} 

AFFILIATIONS

¹Indian Institute of Science Education and Research, Pune 411008, India

²Tata Institute of Fundamental Research, Hyderabad 500107, India

³Indian Institute of Technology Hyderabad, Kandi 502285, India

^{a)}ramgopal@tifrh.res.in

^{b)}vsharma@iith.ac.in

ABSTRACT

Molecules ionized by intense (10–100 TW/cm²) and ultrashort (tens of femtoseconds) laser fields undergo rotation and alignment mediated through their polarizability. The expected alignment is indeed observed in the case of O₂ molecules ionized by intense laser pulses of 800 nm wavelength and 25 fs duration, as observed through velocity imaging of the fragments. Strikingly, when 35 fs pulses of 400 nm wavelength of comparable intensity are employed, an anomalous hindering of this alignment is observed. In both cases, we propose dissociation pathways for the energetic ions consistent with the recorded kinetic energy distributions. Using a semiclassical model of induced rotation of the molecular ion that involves polarizabilities of the participating excited states, both behaviors are reproduced. The model suggests that the difference in the observations can be attributed to a transient negative polarizability in an intermediate state of the proposed pathway.

Published under license by AIP Publishing. <https://doi.org/10.1063/1.5130706>

I. INTRODUCTION

The tendency of a charge distribution to rearrange itself in response to an external electric field is quantified by its polarizability. The polarizability of a molecule manifests itself in the response, for instance, to an intense laser field. In an intense (10–100 TW/cm²) laser field, a molecule is ionized via tunneling through the potential barrier resulting from the combination of the external field and the mean field of the nuclei.^{1,2} Field induced coupling of the parent electronic state with dissociative excited states leads to fragmentation. For example, O₂ is ionized in a linearly polarized ultrashort (<100 fs) moderately intense (~10¹³ to 10¹⁵ W/cm²) laser field through strong field tunnel ionization.² This can be represented as an adiabatic Franck-Condon (FC) type transition from the ground state O₂ [Fig. 1(b)]. The resultant O₂⁺ is predominantly populated in either its ground state X²Π_g or the excited state a⁴Π_u.^{3–6} Despite the ordinarily bound nature of these parent molecular ion states, dissociation may occur through laser-induced coupling with higher excited states. To illustrate, in the Floquet representation¹ shown in Fig. 1(c), an excited state A²Π_u

is “red-shifted” (or “laser dressed”) by five photon energies, 5ω, resulting in a crossing with the X²Π_g state. Ions in the parent state (X²Π_g), with populated vibrational levels above this crossing and over the dissociation limit of the dressed A²Π_u state, will dissociate into the fragments O (³P) and O⁺ (⁴S⁰). The direction of ejection of the fragments is influenced by the rotational impulse provided by the trailing part of the laser pulse, the so-called postionization alignment.⁷ With increasing laser intensities, the observed fragment distribution usually tends to peak along the polarization axis,^{8,9} illustrating alignment. Experimental ion velocity or momentum data, combined with computations, give access to the polarizability of excited states of the molecular ion. We may consider the O₂⁺ molecular ion subjected to a (cycle-averaged) laser field E(t). Its rotational response to the field, treating it to be a nonrigid rotor, is given by the equations^{7,10}

$$\mu\ddot{R} = -\frac{\partial V(R)}{\partial R}, \quad (1)$$

$$\ddot{\theta} = -\Delta\alpha\frac{E^2(t)}{2I}\sin(2\theta) - 2\frac{\dot{R}}{R}\dot{\theta}, \quad (2)$$

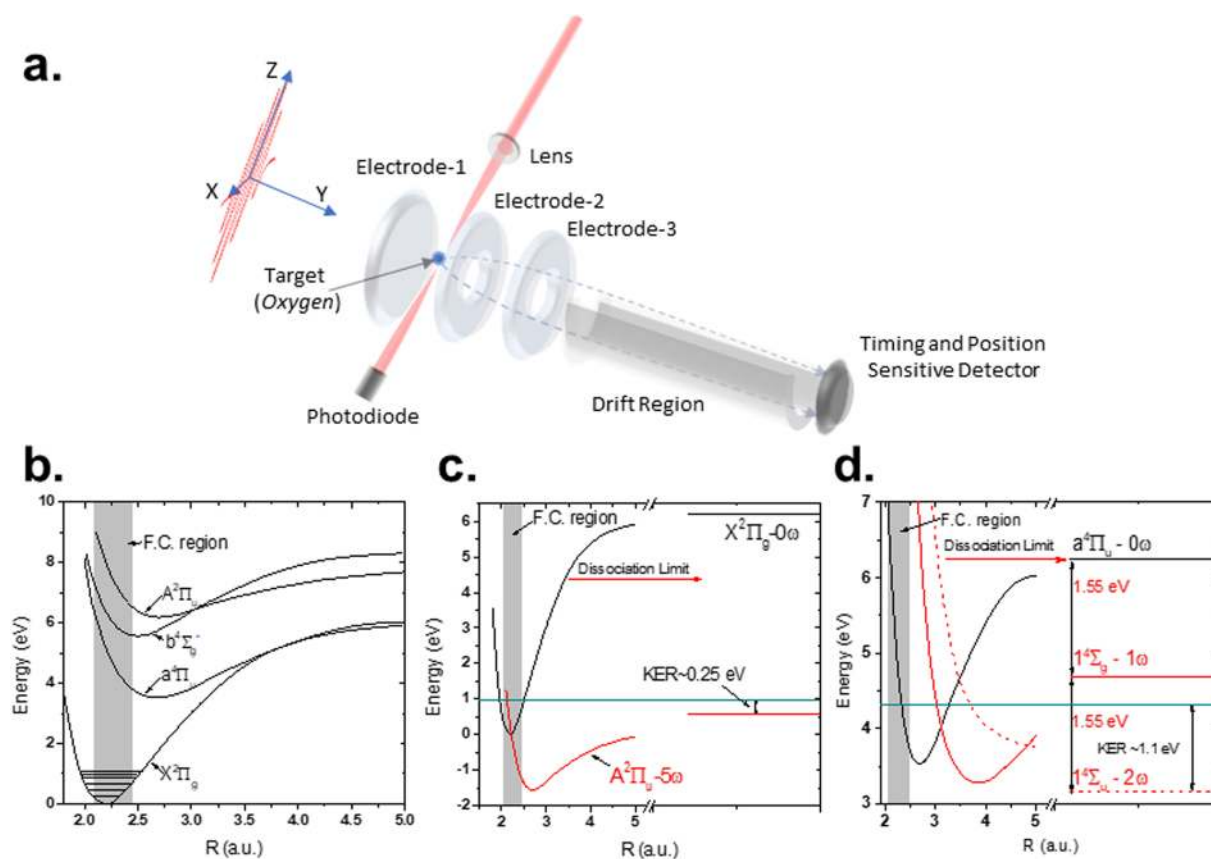


FIG. 1. Molecular ionization and dissociation in strong laser fields studied using an ion imaging spectrometer. (a) Intense laser pulses ionize and fragment the molecule. The ion imaging spectrometer uses electric fields to map the velocity of dissociating fragments to position, captured by using a detector. The ionization and dissociation can be viewed as follows: Shown in (b) are the potential energy curves of the ground state of O_2^+ and the low lying excited electronic states of O_2^+ . The x-axis is the internuclear separation R in atomic units (a.u.), and the gray shaded boundary shows the Franck-Condon region. Possible dissociation channels through the ground state $X^2\Pi_g$ (c) and (d) the first excited state $a^1\Pi_u$ are shown. These states can dissociate through a light-induced coupling (red curves) with higher-lying states. The green solid line in both the plots shows the vibrational level with the largest Franck-Condon factor.

where R is the internuclear separation, θ is the angle made by the internuclear axis with respect to the laser polarization, μ is the reduced mass of the molecule with a moment of inertia I , and $V(R)$ is the potential energy of the molecular ion as a function of the internuclear separation. $\Delta\alpha$ is the polarizability anisotropy of the molecule, given by $\alpha_{\parallel} - \alpha_{\perp}$, where α_{\parallel} and α_{\perp} are the molecular polarizabilities along the internuclear axis and perpendicular to it. These equations predict impulsive angular acceleration (i.e., a “rotational kick”) toward the laser polarization axis if the polarization anisotropy is positive, which is the norm in the molecular alignment.¹¹ If $\Delta\alpha$ is negative, it may be possible to observe an antialignment. When $|\alpha_{\perp}| \ll |\alpha_{\parallel}|$, a large negative polarizability anisotropy requires $\alpha_{\parallel} < 0$, a condition that cannot be met if the molecular alignment involves only the ground state.¹¹

In this paper, we examine strong field ionization followed by dissociation of O_2 by intense ultrashort laser pulses at two wavelengths, 800 nm and 400 nm. Using three-dimensional velocity map imaging, the obtained angular distribution of the fragments using 800 nm laser pulses confirms the alignment of the O_2^+ molecular

ion toward the laser polarization axis during dissociation. We formulate a semiclassical model based on the above equations, which includes quantum chemistry calculations of static polarizability of the involved molecular ion states. We follow the dynamics of dissociation and rotation and explain the observed alignment through the calculated positive polarizability of the parent molecular ion state. Intriguingly, when 400 nm laser pulses are used in the experiments, this alignment is seen to be impeded. The same model also explains this new observation, suggesting that a transient negative polarizability in the coupled dissociating state frustrates the induced alignment. These results prompt further investigation into this apparent hindering of the rotation to be explored over different intensity and pulse duration regimes.

II. EXPERIMENTAL METHOD

A. Laser specifications

A Femtopower V (Spectra-Physics, Austria) laser generates 25 fs, 1 kHz, and 5 mJ pulses at 800 nm. Some of the energy is

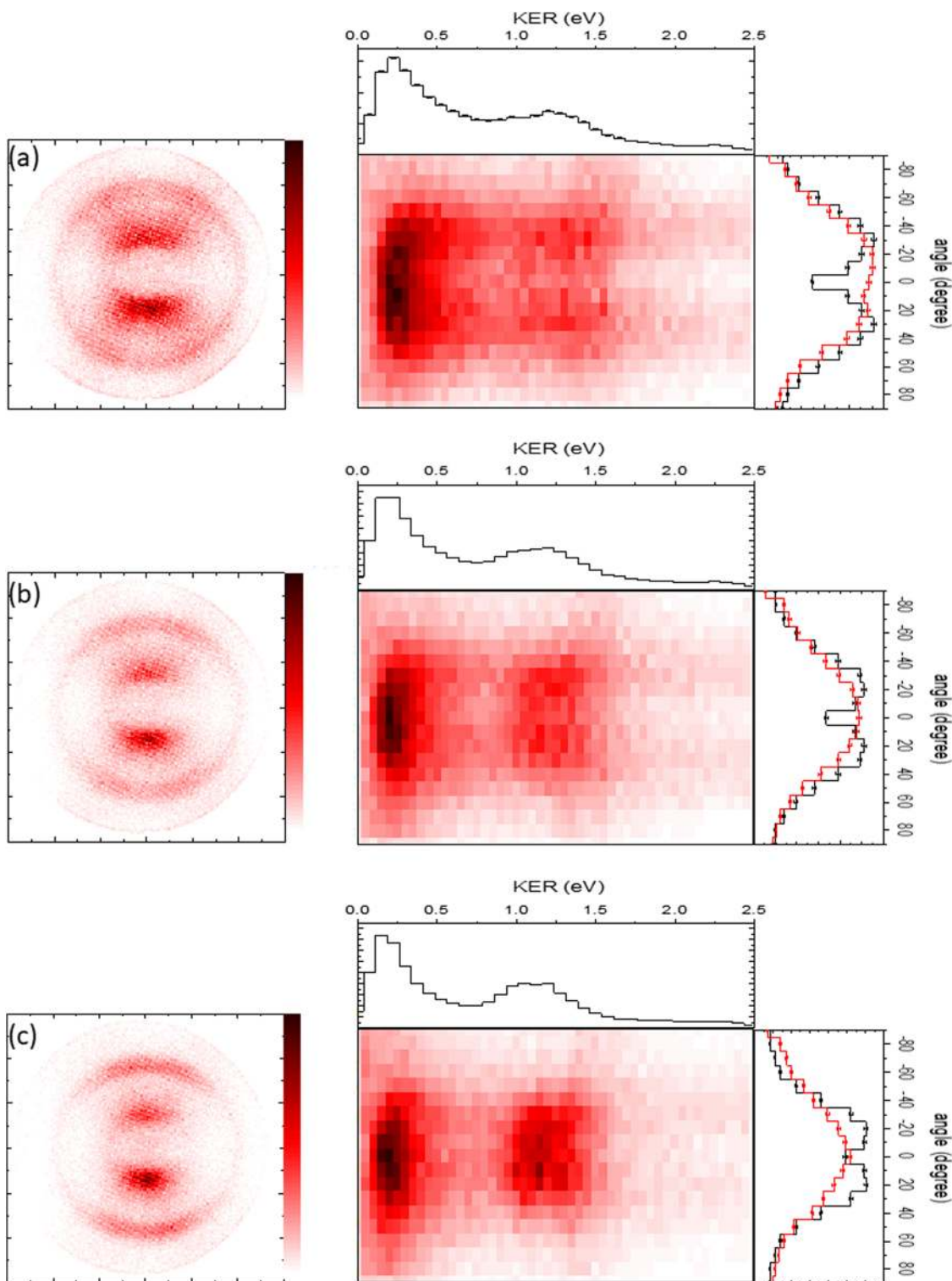


FIG. 2. Velocity slice maps of O^+ ion fragments in the plane of the laser polarization for 800 nm, 25 fs pulses at (a) $2I_0$, (b) $3I_0$, and (c) $4I_0$. Position and intensity scales are in arbitrary units. Corresponding KER- θ plots are in the middle panel. Angular distributions (with the laser polarization axis as the reference) of the high energy ions (0.8–1.3 eV) are shown in the extreme right panel in black. The corresponding distribution for the low energy ions (<0.8 eV) is plotted in red.

used to produce 35 μJ of 400 nm pulses by second harmonic generation using a 0.5 mm thick KDP crystal (Eksma Optics, Lithuania). Appropriate filters are used to separate out the remnant fundamental laser radiation. The polarization of the laser beam is linear and is set perpendicular to the spectrometer axis using a thin $\lambda/2$ plate (B-Halle, Germany). A thin $f = 30$ cm lens focuses the laser to a spot size (the diameter at half-maximum) of 70 μm , which is also used to estimate the peak intensity ($I_0 = 2.3 \times 10^{13}$ W/cm²). The pulse duration immediately after the laser amplifier is measured through autocorrelation and estimated at the spectrometer by accounting for dispersion along the beam path. The maximum intensity used for 800 nm is $4I_0$ and that for 400 nm is $3I_0$. These upper limits are chosen such that no O_2^+ is observed in the spectrometer. At the highest laser intensity used, the count rate for the parent molecular ion O_2^+ is around 1 kHz or one ion generated per laser pulse, ruling out space charge effects by ions generated in the laser focal volume.

B. Velocity map imaging technique

Laser pulses are focused on an effusive jet of O_2 inside a vacuum chamber. An ion imaging spectrometer¹² is used (see Fig. 1) to collect the fragmented ions created by the laser pulse. The ion lens optics maps equivelocity ions of a given species (mass-to-charge ratio) to the same radius on a planar detector. The detector is a microchannel plate (MCP) backed by a delay line-type position sensitive anode (Roentdek GmbH, Germany) and provides the two dimensional position and flight time of each ion. The flight times are with reference to the laser pulse, the start signal being obtained from a fast photodiode (DET10A Thorlabs, USA). Time and position information of each hit is saved in the list mode format. Data were acquired for about 2 h at each experimental setting. In post-experiment processing, events with flight times close to the mean arrival time of the O^+ ions were selected, thus choosing ions with a nearly zero velocity component perpendicular to the laser polarization axis.¹² These velocity slice images are presented in Figs. 2 and 4. Each position corresponds to a unique velocity of the ion, thereby allowing us to obtain a 2D map of velocity distribution of the fragmented ions ejected in a plane containing the laser polarization axis. Since events lying on a circle centered on the 2D map correspond to ions having the same magnitude of velocity, the kinetic energy spectrum of the ions is readily obtained by integrating the counts over the azimuthal angle at each radius. The Kinetic Energy Release (KER) spectrum can be further calculated, since the momentum of the neutral O fragment is equal and opposite to that of O^+ . The multihit capability¹² of the detector (up to 8 ions with a double hit dead time of <10 ns) is also exploited to check if there are any coincident O^+ ions recorded in the second hit. This allows us to establish that the ions recorded are from the dissociation channels (O^+/O) and not from any Coulomb explosion channel (O^+/O^+). Calibration of the spectrometer has been discussed in a previous paper.¹²

III. RESULTS

A. Observed O^+ distributions

1. For 800 nm laser pulses

The left panel of Fig. 2 shows the velocity maps of the O^+ ion at three different values of laser intensities ($2I_0$, $3I_0$, and $4I_0$). The

middle panel shows a two dimensional density representation of the same data with KER on the x-axis and θ (with respect to the laser polarization) on the y axis. In all spectra, two distributions corresponding to O^+ ions of different energies peaking at 0.25 eV and 1.2 eV, respectively, are easily identifiable. A weak peak around 0.5 eV is also seen, which decreases in strength with increasing laser intensity.

The highest density of energetic (1.2 eV) O^+ ions is not along the direction of the laser polarization axis. This is not entirely unexpected, as the molecular tunnel ionization rate depends on the angle between the molecular axis and the laser polarization. In a quasi-static tunneling picture of strong field molecular ionization, the ionization rate is the highest when the direction of the laser polarization axis is along the region having the highest probability of finding an electron. In ionization of molecules having the highest occupied molecular orbital (HOMO) of π symmetry (e.g., O_2 and CO_2), the consequence of this preference is evident. Previous experiments^{13–16} and theory⁷ (Molecular Orbital-Ammosov Delone Krainov, MO-ADK) have shown that the ionization probability for O_2 peaks for molecules aligned around 40° [as in the red dashed curve in Fig. 3(a)] with respect to the laser polarization axis, which is when the HOMO orbital overlaps with the laser polarization axis. Here, at the lowest intensity, the angular distribution of the energetic ions (black in the right panel) peaks at an angle of 30° , shifting toward 20° at the highest intensity. Concomitantly, the mean of the distribution shifts from 38° to 28° and the standard deviation shows nearly no change. The detector angular resolution is $\approx \pm 1.5^\circ$ for the high energy ions not taking into account thermal and laser focal volume contributions. The low energy ion distribution is also not strongly peaked along the laser polarization axis at low intensities. But with increasing intensity, these ions also tend to appear predominantly along the laser polarization axis. Quantitatively, however, the mean of the distribution is within $30^\circ \pm 1^\circ$, and a prominent alignment as observed for the energetic ions is not seen. The low resolution of the detector for the low energy ions ($\approx \pm 3^\circ$) precludes a finer distinction of the angular distribution behavior with intensity.

To establish a pathway for the high energy ions, we turn to the peak positions in the KER distribution, as illustrated in Fig. 3. As the laser intensity is just at the threshold for dissociative ionization, we consider only single-photon coupling between the O_2^+ ground state and the dissociative state. Molecular dipole selection rules restrict the states which can couple, thereby limiting the number of pathways to only a few.

With these restrictions, the possibility of dissociative ionization by populating first the $\text{O}_2^+ X^2\Pi_g$ state, followed by coupling to a dissociative state of O_2^+ is ruled out, since the second step in this process would also require multiphoton coupling. The laser parameters in the present experiment rule out this possibility. The $\text{O}_2^+ a^4\Pi_u$ is the next energetically available state. Ionization to this state, followed by a single-photon transition to a dissociative state is possible, giving the dissociation pathway for events with KER ≈ 1.2 eV as $\text{O}_2^+ |a^4\Pi_u\rangle \rightarrow |1^4\Sigma_g^+ - 1\omega\rangle \rightarrow |1^4\Sigma_u^+ - 2\omega\rangle$, which is depicted in Fig. 3(e).

A similar analysis for the low energy ions is not straightforward. Multiple dissociation pathways can contribute to the prominent low energy KER peak (0.25 eV) in Fig. 3(d). For example, again considering one photon mediated dissociation pathways alone,

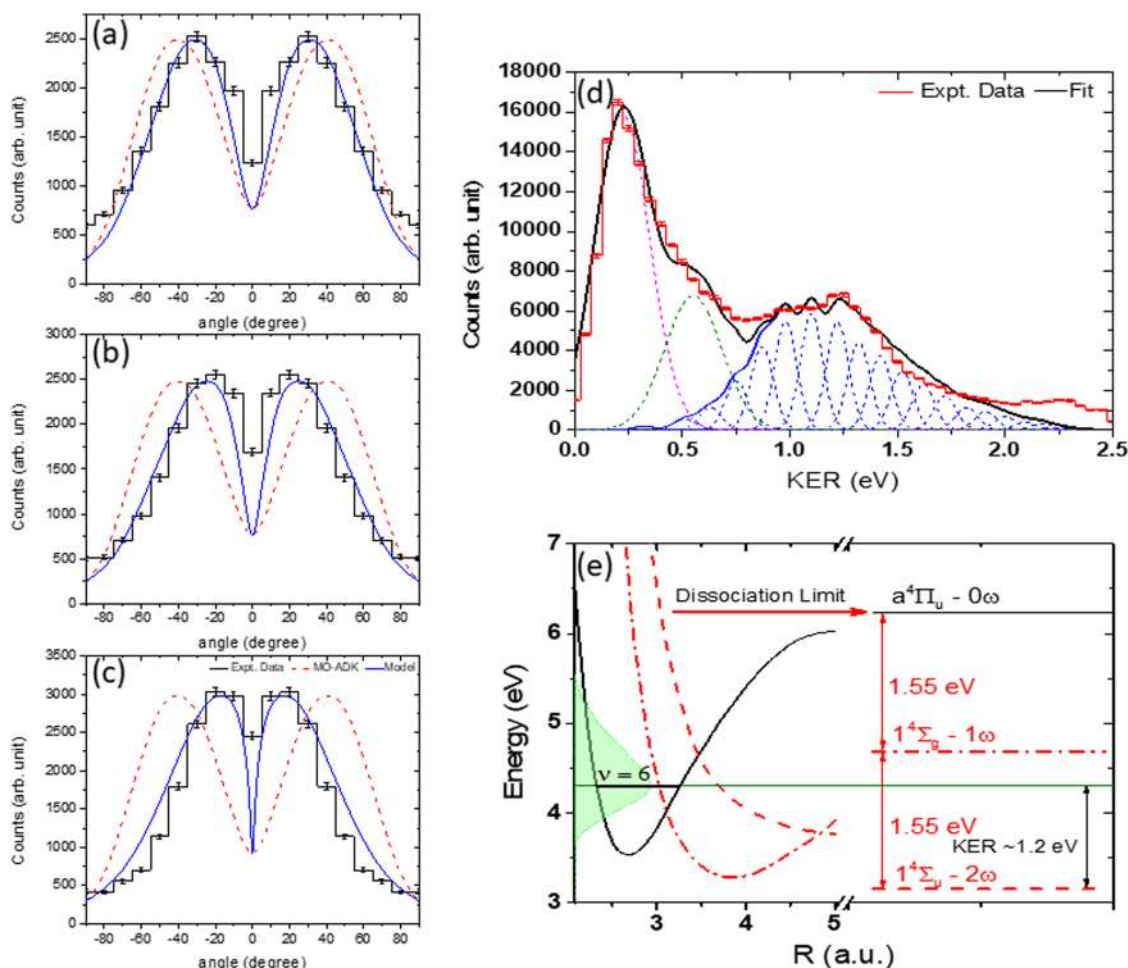


FIG. 3. The angular distribution (with the laser polarization axis as the reference) of the high energy ions is shown for (a) $2I_0$, (b) $3I_0$, and (c) $4I_0$. Black histograms are experimental data, and the red dashed curve is the distribution expected from molecular tunneling theory. The blue solid curve is from our model that includes molecular tunneling and angular acceleration by the laser. (d) The measured KER spectrum (red histogram) of the O_2^+ molecular ion for 800 nm at $2I_0$ is compared with the expected KER distribution (blue curve) from the dissociation channel $|a^4\Pi_u\rangle \rightarrow |1^4\Sigma_g^- - 1\omega_u\rangle \rightarrow |1^4\Sigma_u^+ - 2\omega\rangle$. The pink and green dashed curves are fits to peaks at KER of 0.25 and 0.5 eV, respectively. The black curve is the combined expected KER spectrum. (e) The proposed dissociation channel for 800 nm pulses. The filled green area shows the population in the vibrational levels of O_2^+ $a^4\Pi_u$ state. The shape of the KER spectrum in (d) is arrived at by convolving the vibrational levels (blue dotted) weighted by their corresponding Frank-Condon coefficients.

$|a^4\Pi_u\rangle \rightarrow |f^4\Pi_g - 1\omega\rangle$, $|b^4\Sigma_g^-\rangle \rightarrow |c^4\Sigma_u^- - 1\omega\rangle$, and $|b^4\Sigma_g^-\rangle \rightarrow |2^4\Pi_u - 1\omega\rangle$ are probable pathways which may contribute to the low energy peak at 0.25 eV. Dissociation through the ground state of O_2^+ through (a) $|X^2\Pi_g\rangle \rightarrow |A^2\Pi_u - 1\omega\rangle \rightarrow |^2\Sigma_g^+ - 2\omega\rangle$ or (b) $|X^2\Pi_g\rangle \rightarrow |^2\Sigma_u^+ - 1\omega\rangle \rightarrow |^2\Sigma_g^+ - 2\omega\rangle$ are also possible routes to the low energy ions.⁵ However, this requires that the higher vibrational states of $v \geq 16$ be populated in the FC transition in the ionization, which is improbable. Thus, analysis of the low energy ions is complicated, and in the absence of more information, extracting the most probable pathway is futile.

2. For 400 nm laser pulses

Figure 4 shows the two dimensional velocity distribution (in a plane containing the laser polarization axis) with 400 nm, 35 fs

laser pulses at the intensities I_0 , $2I_0$, and $3I_0$. In Fig. 4(a), two concentric distributions corresponding to O^+ ions of different energies are identifiable. The inner, low energy, ion distribution appears to consist of peaks at KER of 0.25 eV and 0.5 eV. The angular distributions corresponding to the low energy (red) and energetic ions (1.1 eV, black) are shown in the right panel of Fig. 4. The peak of the observed angular distribution for the energetic ions is at $\approx 25^\circ$ for all intensities and is in disagreement with the prediction [$\sim 40^\circ$, red dashed curve in Fig. 5(a)] of the molecular tunneling theory.² The mean of the distribution stays at 34° , and likewise, the standard deviation shows no change with increasing laser intensity. The low energy ions do not have a prominent dip along the laser polarization axis compared to the high energy ions. The mean angle of ejection at low intensities is 28° which increases to 33° at $2I_0$

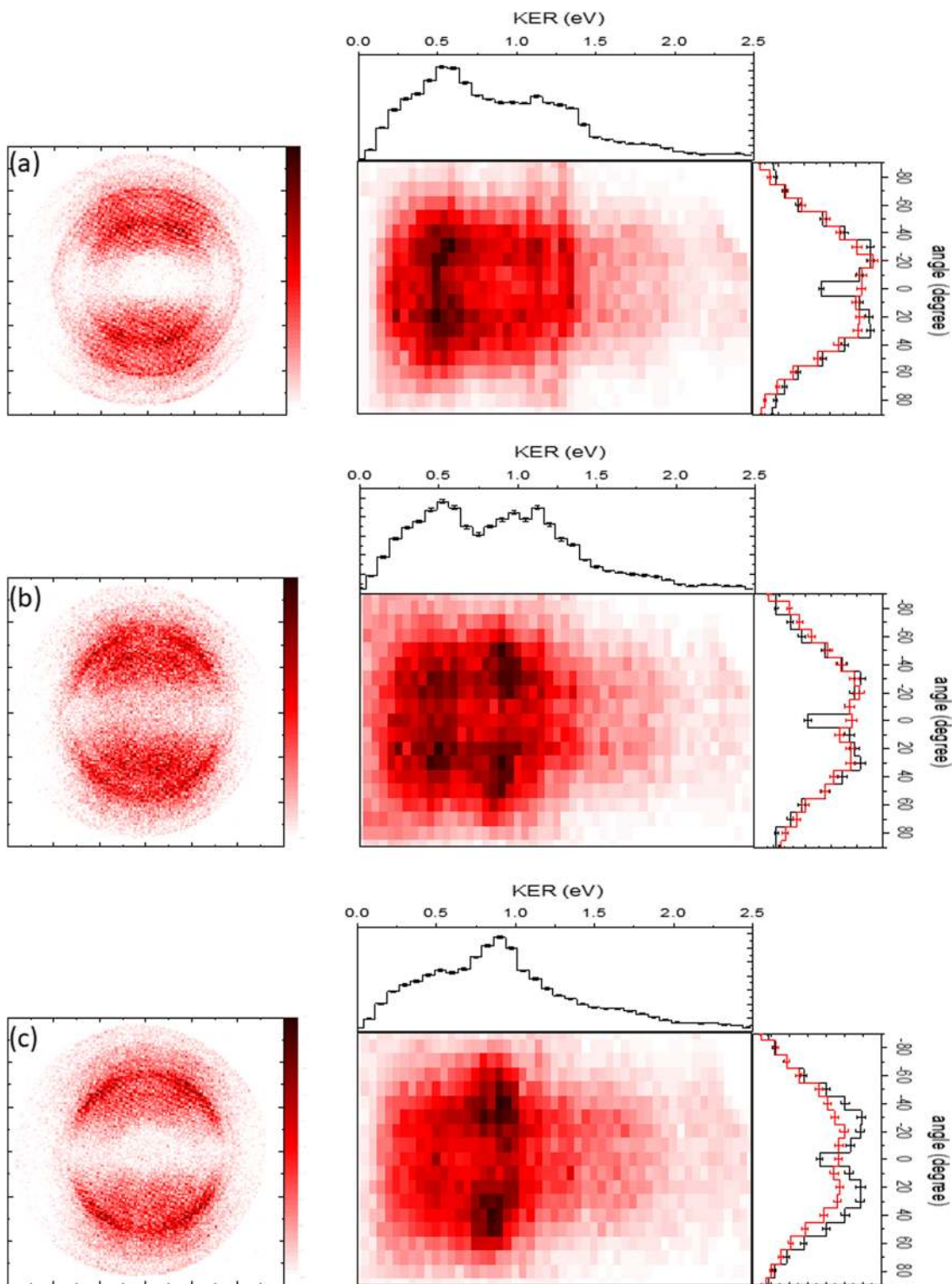


FIG. 4. Same as Fig. 2, but for 400 nm, 35 fs pulses at (a) I_0 , (b) $2I_0$, and (c) $3I_0$.

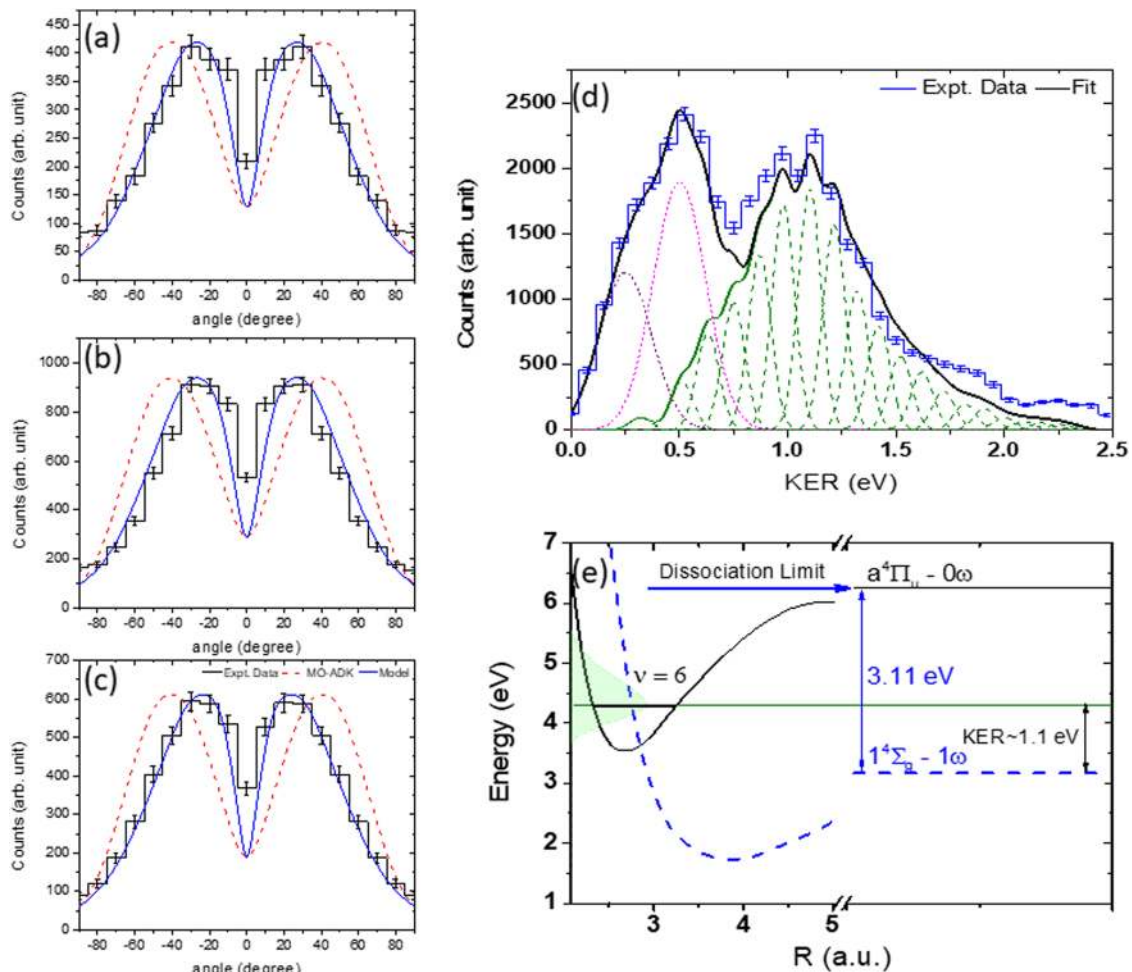


FIG. 5. Same as Fig. 3, but for 400 nm at intensities of (a) I_0 , (b) $2I_0$, and (c) $3I_0$. (d) KER spectrum of the O_2^+ molecular ion for a 400 nm laser pulse at $2I_0$. The blue experimental histogram is fitted with the proposed dissociation channel (green) $|a^4\Pi_u\rangle \rightarrow |1^4\Sigma_g^+ - 1\omega\rangle$ and peaks at 0.25 eV and 0.5 eV. In (e), the dissociation channel is schematically depicted.

and falls to 31° for $3I_0$ with no significant change in the standard deviation.

We apply the same considerations in determining the pathway for the 400 nm case as in the case of 800 nm. The plausible pathway under 400 nm irradiation is $O_2^+ |a^4\Pi_u\rangle \rightarrow |1^4\Sigma_g^+ - 1\omega\rangle$ for the KER peak at 1.1 eV (Fig. 5). In other experiments with 400 nm laser pulses, KER peaks at 0.6 eV (Ref. 3) and 0.7 eV (Ref. 5) have been identified with the pathway $O_2^+ |a^4\Pi_u\rangle \rightarrow |f^4\Pi_g - 1\omega\rangle$. However, in addition to the difference in the peak energies, the angular distributions observed here are significantly different in comparison. Once again, it is difficult to assign a unique dissociation pathway for the prominent low energy (KER peak 0.5 eV) ions. $O_2^+ |a^4\Pi_u\rangle \rightarrow |2^4\Pi_g^+ - 1\omega\rangle$, $O_2^+ |b^4\Sigma_g^-\rangle \rightarrow |3^4\Sigma_u^+ - 1\omega\rangle$, and $O_2^+ |b^4\Sigma_g^-\rangle \rightarrow |3^4\Pi_u - 1\omega\rangle$ are examples of possible pathways leading to these ion energies for the O^+ fragments. Furthermore, as shown in Fig. 5(d), there is a significant overlap of the dissociation channel $|a^4\Pi_u\rangle$

$\rightarrow |1^4\Sigma_g^+ - 1\omega\rangle$ with the 0.5 eV peak. With changing intensities, the Stark effect also modulates the observed vibrational distributions. This could account for the shifting of the 1.1 eV peak toward 0.9 eV with increasing laser intensity in Fig. 4. A similar shift is seen even for the 800 nm laser data. However, in the 400 nm case, this changing distribution would imply a larger contribution of this pathway to the low energy ions.

So, within the limitations of the experiment and dissociation pathway assignments, it is clear that an interpretation of the observations can be attempted unambiguously, only, for the high energy ions ≈ 1.1 – 1.2 eV for 800 nm and 400 nm laser data. Qualitatively, for the 800 nm case, the angular distributions appear to agree with the model of tunnel ionization followed by postionization alignment. For the 400 nm case, in complete contrast to the 800 nm case, the angular distribution is unaffected by the increasing laser intensity. The difference is only in

the relative intensities of the low energy and high energy ions. At first glance, the latter observations seem to be in complete disagreement with the postionization alignment model, at least qualitatively.

IV. POST IONIZATION ROTATION MODEL

To make a quantitative correspondence with the postionization alignment model requires us to dynamically account for a number of parameters. These include the Potential Energy Curves (PECs)

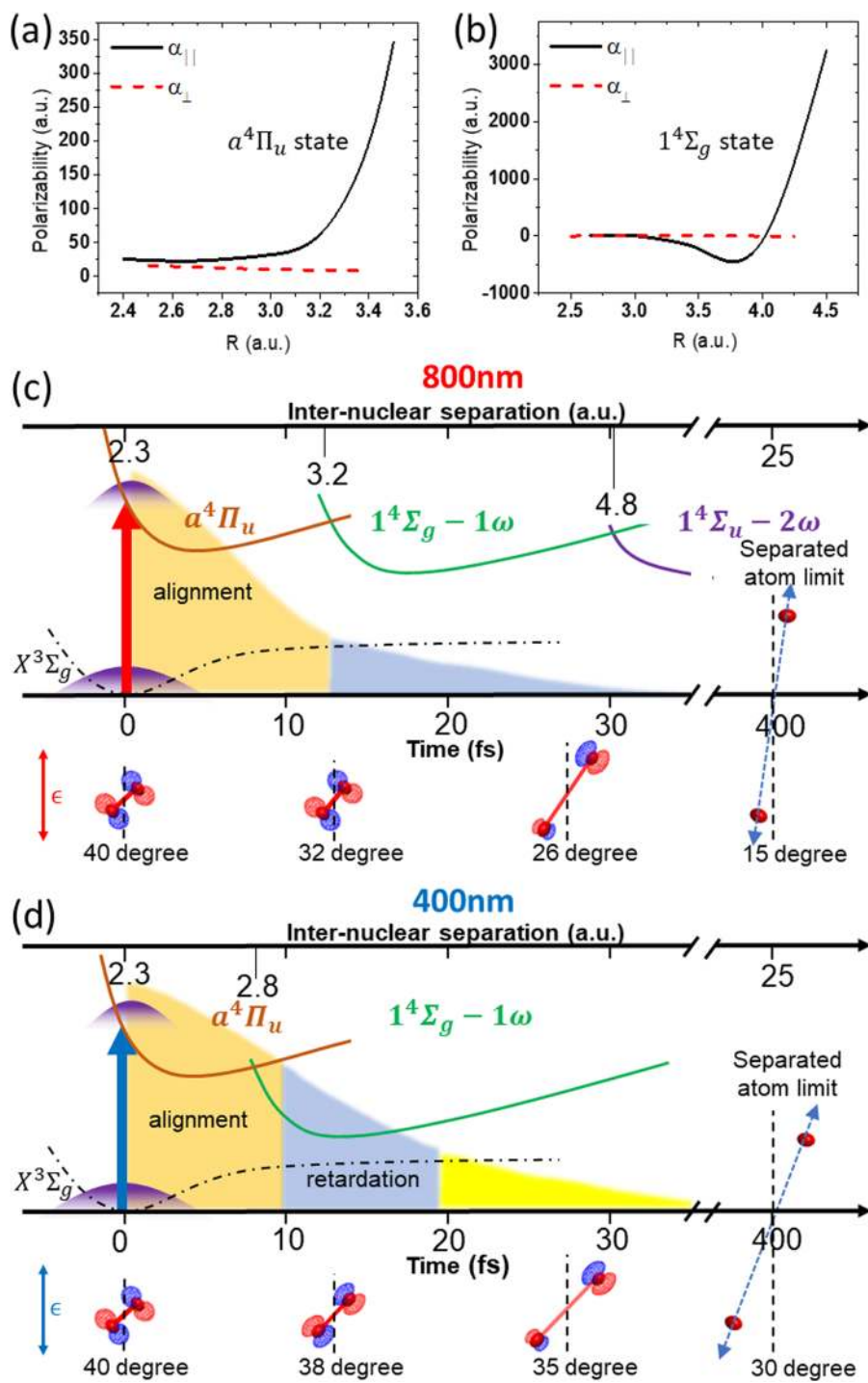


FIG. 6. [(a) and (b)] Calculated polarizabilities ($|\alpha_{\perp}|$ and $\langle\langle\alpha_{||}\rangle\rangle$) of the $\alpha^4\Pi_u$ and $1^4\Sigma_g^+$ states which participate in the dissociative ionization. [(c) and (d)] Schematic of the dissociation of O_2^+ . For 25 fs, 800 nm laser pulses, $\alpha_{||} > 0$ of the parent molecular ion state (brown curve) imparts a strong aligning torque. The shaded areas denote the cycle-averaged, quasistatic field of the laser pulse. When the ion makes a transition to the negative polarizability state (green curve) at $R \sim 3.2$ a.u. ($t \sim 13$ fs), the trailing pulse intensity (blue shaded) is not sufficient to counter the alignment. For 35 fs, 400 nm laser pulses, the ion crosses over to the $\alpha_{||} < 0$ state earlier in time at $R = 2.8$ a.u. ($t \sim 7$ fs), and with sufficient remnant laser intensity (blue shaded), the alignment is hindered.

of the states involved in the dissociation of the molecular ion, the polarizability of these involved states, the laser pulse duration and its intensity, and the initial orientation of the molecular ion with respect to the polarization axis. The pulse durations and intensities can be obtained from the experimental estimations. Additionally, we postulate that the molecular ion is formed at the peak of the laser pulse envelope and that the initial orientation of the molecular ion is fixed by molecular tunneling theory.⁷ What remains to be determined is the polarizability of the molecular ion as the molecule dissociates. If the dissociation pathway is assigned, in other words the participating electronic states are identified, the polarizability can be extracted through quantum chemistry calculations. In this section, we have confined ourselves to analyzing the high energy ions for both 800 nm and 400 nm results as we can assign unique pathways for these fragments. It is to be noted that this model ignores the effect of molecular alignment prior to ionization, the well-known dynamic alignment.¹¹ This is justified⁷ for ultrashort laser pulses and particularly in the case of O₂ which has negligible polarizability anisotropy in the neutral ground state as known from previous works¹⁷ and confirmed by our calculations.

A. Calculation of polarizabilities

The static dipole polarizability (α_{\parallel} and α_{\perp}) of the molecular ion is calculated at various internuclear separations R for each of the participating states. The energy of the molecular ion is first calculated in the presence of a static electric field and the polarizability is then obtained as the second order derivative of the energy with respect to the electric field. Calculations of the energies, with and without the static field, have been performed using the GAMESS¹⁸ suite of programs. The multiconfiguration (MC) self-consistent (SCF) method along with the configuration interaction (CI) has been used to obtain the excited state potential energy (PE) curves. The consistency of the calculations has been cross-checked by using four different basis sets to calculate the PE curves. The four basis sets used are Dunning and Hay type double zeta basis set with d - and p -type polarization functions and Dunning type correlation consistent triple zeta valence basis augmented with a set of diffuse functions (aug-cc-pVTZ). The obtained PE curves of the quartet states match well with the previous reports.¹⁹

Classical temporal evolution of the internuclear separation along the potential energy curves (PECs) using Eq. (1) is used to extract $\Delta\alpha$ at each time step. The calculated polarizabilities for the states $a^4\Pi_u$ and $1^4\Sigma_g^+$ are plotted in Fig. 6 as a function of R . For small internuclear distances, the values for both states are small and positive. Beyond R of 3.0 a.u., the polarizability of $1^4\Sigma_g^+$ goes negative. Conversely, the polarizability of the $a^4\Pi_u$ state rapidly rises to large positive values with increasing R .

B. Rotation and alignment of the transient molecular ion

As discussed earlier, the shape of the HOMO of O₂ determines the preferred orientation of O₂ for ionization. The molecular ion is assumed to be created at the temporal peak of the laser pulse at an internuclear separation of $R_0 = 2.3$ a.u. via a Frank-Condon transition. At the peak of the laser pulse, $t = 0$, the molecular ion is created in the $a^4\Pi_u$ state with $R = 2.3$ a.u. In this state, the molecule is

“kicked” in the direction of the laser polarization axis by the induced dipole, resulting in alignment.

The coupling of the polarizability to the averaged electric field of the laser pulse [Eq. (2)] accounts for the rotational impulse, causing the molecule to change its orientation. Since the rotor is nonrigid, the rotational acceleration also leads to an increase in the internuclear separation. This, in turn increases the moment of inertia thereby damping the rotational motion. This evolution of the system is followed in time until the internuclear separation increases to 10 times the ground state bond length, giving us the asymptotic value of the molecular orientation. This calculation is done for different initial molecular orientations between $\theta = 0^\circ$ and 90° and weighted by angle dependent ionization probability from MO-ADK.² In a quantum mechanical picture, the above process can be modeled as the evolution of a rovibrational wavepacket²⁰ created in the $a^4\Pi_u$ state. The wavepacket evolves leading to increasing mean internuclear distance with time corresponding to a classical traversal of the molecule along the PEC. This is shown schematically in Fig. 6.

The differentiation between the responses to 800 nm and 400 nm irradiation hinges on the difference in the point of crossover from one state to another. The transition in the 800 nm case happens at $R \sim 3.2$ a.u. and at $R \sim 2.8$ a.u. in the 400 nm case. Thus, in the 400 nm case, the molecular ion crosses over to the $1^4\Sigma_g^+$ state at an earlier instance in time as compared to the 800 nm case. The longer 400 nm pulse means that after the molecular ion makes a transition to the $1^4\Sigma_g^+$ state, the negative polarizability produces a decelerating torque, hindering the alignment. In the 800 nm case, by the time the transition to the $1^4\Sigma_g^+$ state occurs, the laser intensity falls drastically, and as a result, the rotation under the influence of the positive value α_{\parallel} of the $a^4\Pi_u$ state continues essentially unhindered.

The blue curves in the angular distributions shown in Figs. 3 and 5 are from calculations based on the evolution along the pathways explained above and the calculated polarizabilities of the participating states. The only free parameter used in the model is the laser intensity and the calculated angular distributions are normalized to the experimental distributions on the total counts. The intensities used for the calculation are systematically higher than the experimental intensities by a nearly constant factor of around 1.5. A 20%–25% uncertainty in estimating experimental laser intensities is a common issue in strong field laser matter interaction studies, so the broad agreement between the model and the experiment is noteworthy.

V. DISCUSSION

In essence, we have inquired why fragment angular distributions and their dependence with laser intensity are different for 800 nm and 400 nm laser pulses. In the two step model for the dissociation, we have assumed, the ionization of the molecule is through a tunneling process and yields a preferred alignment for the molecule. In the second step, the dissociation of the molecular ion proceeds through dressed states whose polarizabilities account for further rotation of the molecular ion during dissociation. The tunnel ionization has been modeled through MO-ADK here, but it is pertinent to have a look at other approaches used to explain the angular distribution from fragmentation. For example,

including multiorbital tunneling²¹ in the ionization from N₂, O₂, and CO in the calculations, angular dependent ionization rates can also be obtained. These compare better with experimentally obtained angular distributions following the Coulomb explosion in laser induced double ionization of these molecules. However, it is clear that for the intensities in the range of 10¹⁴ W/cm², the main contribution to the angular distribution is from the HOMO for molecules such as D₂, N₂, and O₂, while for CO, there is significant ionization from the HOMO-1 orbital. The peak for angular distributions for O₂, for example, is $\geq 35^\circ$, as compared to 40° using MO-ADK theory. Using Time Dependent Schrödinger Equation (TDSE) calculations,^{22,23} the ionization yields from the HOMO orbital for O₂ ($1\pi_g$) are seen to be greater than those from the HOMO-1 ($1\pi_u$) orbital by more than four orders of magnitude for molecules aligned at 45° to the laser polarization (800 nm). Along the laser polarization axis, ionization from the HOMO-2 ($3\sigma_g$) becomes comparable to, or even greater than that from the HOMO-1. This would yield an ion signal component along the laser polarization axis and could become relevant for the interpretation of the 800 nm data. However, the ionization rates for the HOMO-2, along the laser polarization axis, are still two orders of magnitude lower than those of the HOMO for 400 nm and four orders of magnitude lower for 800 nm. Furthermore, including other effects such as exchange interactions²⁴ would lead to small corrections to the absolute value of the peak of the angular distribution of O₂⁺ and to corrections in the yield parallel and perpendicular to the laser polarization axis.

In the dissociation step, laser field induced deformation of the PEC manifests as bond-softening and bond-hardening, resulting in preferential directions of ejection of the fragments.²⁵ Specifically, in bond softening, the bond is weakened and dissociation through this channel is enhanced for transition dipole moments aligned parallel to the laser polarization axis. This could be a possible explanation for the alignment trend observed for the 800 nm data. However, to explain the 400 nm results, we would have to invoke the opposite effect of bond-hardening, where the molecular ion seeks antialignment to dissociate, with the additional complication of having to account for the absence of the bond-softening channel in the experimental data. We have considered these possibilities with the molecular ion states available and have not been able to come to consistent and physically feasible explanations.

The observation of alignment effects in laser induced fragmentation of molecules is fairly ubiquitous over a large range of laser intensities and pulse lengths. Only with intense ultrashort (<8 fs) laser pulses where Coulomb explosion of the doubly charged species is initiated before the molecule can rotate is the alignment arrested. The experimental angular distribution of O⁺ in these experimental conditions matches with MO-ADK predictions. Our results of the 800 nm pulses appear to match the MO-ADK predictions in conjunction with the postionization alignment model. In the case of 400 nm, primarily, we notice a discrepancy with respect to the expected angular distribution from MO-ADK alone and also an apparent discrepancy from the postionization alignment model. Through our semiclassical model, we can account for both the alignment and the hindering of alignment in the dissociation step.

A criticism of the model could be the use of static polarizabilities close to the transition. In the region of the resonance, the polarizability associated with the oscillating laser field, i.e., the dynamic polarizability should be considered. However, the dynamic polarizability rapidly diverges and flips its sign as it passes the resonance. Therefore, for the dissociating molecule, the integral contribution to the aligning torque from the dynamic polarizability is insignificant compared to that due to a quasistatic (averaged) field. An ambiguity in interpretation may stem from the assignment of the dissociation pathway, for which we have assumed that only single photon transitions couple O₂⁺ to a dissociating state (subsequent to multiphoton ionization of O₂ in the ground state). These assignments need to be validated with TDSE calculations. Notwithstanding these limitations of our model, we posit that our results suggest that the negative polarizability of an excited state leads to the hindering of the molecular ion alignment in the laser field. Nevertheless, detailed experiments over varied intensities and pulse lengths are warranted to clarify this interpretation.

VI. SUMMARY AND OUTLOOK

In this paper, we report our experiments on the dissociative ionization of O₂ in intense ultrashort laser pulses at 800 nm and 400 nm. The intensities are kept low such that no double ionization of the molecule is observed ensuring dissociation of O₂⁺ through its low lying excited states only. Angular distribution of the fragments is extracted through velocity map imaging of the O⁺ ion. Dissociation pathways are proposed based on the kinetic energy released in the fragmentation for the fast ions. Static polarizabilities of the participating molecular ion states are computed using the GAMESS suite of programs. Finally, the rotational motion of the dissociating O₂⁺ molecular ion under the influence of the trailing laser pulse is calculated and the angular distribution of O⁺ ions is obtained. The observed angular distribution for 800 nm pulses shows alignment of the dissociating molecular ion, which is well understood through the positive polarizability of the parent molecular ion state. When 400 nm pulses are employed, this alignment is hindered. The model explains this new observation: a transient negative polarizability of the intermediate state is responsible for hindering the alignment. These results are a striking illustration of electron correlation phenomena, revealed through dissociation dynamics.

Examples of negative polarizability are sparse, as such phenomena can only be observed in the excited states of the molecule.²⁶ Some reports in this context are on near-threshold photodetachment of alkali ions,²⁷ in which a large negative polarizability of the excited state inhibits the detachment process, and are a consequence of electronic repulsion arising from neighboring low lying electronic states.

A thorough investigation of this singular behavior of O₂⁺ with full quantum mechanical calculations is called for. The state in question is primarily composed of electronic configurations of both antibonding and bonding characters. A subtle change in the relative weights of the configurations under the influence of the electric field causes the state to have higher energy, and hence, the negative polarizability. The involvement of two degenerate or near-degenerate electronic configurations, with a dependence of the relative weights

on the bond-coordinate, suggests a correlation of the nondynamical type. A detailed formal analysis could potentially uncover rich correlation physics.

ACKNOWLEDGMENTS

We thank Professor M. Krishnamurthy for the laser beam time and Dr. R. Ramakrishnan for extending to us the computational facilities of the Tata Institute of Fundamental Research, Hyderabad, and for insightful suggestions. The funding of DST/SERB through Project No. SB/FTP/PS-010/2014 is gratefully acknowledged.

REFERENCES

- ¹J. H. Posthumus, *Rep. Prog. Phys.* **67**, 623 (2004).
- ²X. M. Tong, Z. X. Zhao, and C. D. Lin, *Phys. Rev. A* **66**, 033402 (2002).
- ³A. Hishikawa, S. Liu, A. Iwasaki, and K. Yamanouchi, *J. Chem. Phys.* **114**, 9856 (2001).
- ⁴A. M. Saylor, P. Q. Wang, K. D. Carnes, B. D. Esry, and I. Ben-Itzhak, *Phys. Rev. A* **75**, 063420 (2007).
- ⁵M. Zohrabi, J. McKenna, B. Gaire, N. G. Johnson, K. D. Carnes, S. De, I. A. Bocharova, M. Magrakvelidze, D. Ray, I. V. Litvinyuk, C. L. Cocke, and I. Ben-Itzhak, *Phys. Rev. A* **83**, 053405 (2011).
- ⁶S. De, I. A. Bocharova, M. Magrakvelidze, D. Ray, W. Cao, B. Bergues, U. Thumm, M. F. Kling, I. V. Litvinyuk, and C. L. Cocke, *Phys. Rev. A* **82**, 013408 (2010).
- ⁷X. Tong, Z. Zhao, A. Alnaser, S. Voss, C. Cocke, and C. Lin, *J. Phys. B: At., Mol. Opt. Phys.* **38**, 333 (2005).
- ⁸A. S. Alnaser, S. Voss, X. M. Tong, C. M. Maharjan, P. Ranitovic, B. Ulrich, T. Osipov, B. Shan, Z. Chang, and C. L. Cocke, *Phys. Rev. Lett.* **93**, 113003 (2004).
- ⁹S. Voss, A. S. Alnaser, X.-M. Tong, C. Maharjan, P. Ranitovic, B. Ulrich, B. Shan, Z. Chang, C. D. Lin, and C. L. Cocke, *J. Phys. B: At., Mol. Opt. Phys.* **37**, 4239 (2004).
- ¹⁰C. Ellert and P. Corkum, *Phys. Rev. A* **59**, R3170 (1999).
- ¹¹H. Stapelfeldt and T. Seideman, *Rev. Mod. Phys.* **75**, 543 (2003).
- ¹²R. Gopal, A. Sen, S. R. Sahu, A. S. Venkatachalam, M. Anand, and V. Sharma, *Rev. Sci. Instrum.* **89**, 086107 (2018).
- ¹³I. V. Litvinyuk, K. F. Lee, P. W. Dooley, D. M. Rayner, D. M. Villeneuve, and P. B. Corkum, *Phys. Rev. Lett.* **90**, 233003 (2003).
- ¹⁴M. Meckel, D. Comtois, D. Zeidler, A. Staudte, D. Pavičić, H. C. Bandulet, H. Pépin, J. C. Kieffer, R. Dörner, D. M. Villeneuve, and P. B. Corkum, *Science* **320**, 1478 (2008).
- ¹⁵S. Haessler, J. Caillat, W. Boutu, C. Giovanetti-Teixeira, T. Ruchon, T. Auguste, Z. Diveki, P. Breger, A. Maquet, B. Carré, R. Taïeb, and P. Salières, *Nat. Phys.* **6**, 200 EP (2010).
- ¹⁶C. Vozzi, F. Calegari, E. Benedetti, J.-P. Caumes, G. Sansone, S. Stagira, M. Nisoli, R. Torres, E. Heesel, N. Kajumba, J. P. Marangos, C. Altucci, and R. Velotta, *Phys. Rev. Lett.* **95**, 153902 (2005).
- ¹⁷V. N. C. M. A. Buldakov, *J. Comput. Methods Sci. Eng.* **4**, 237 (2004).
- ¹⁸M. W. Schmidt, K. K. Baldrige, J. A. Boatz, S. T. Elbert, M. S. Gordon, J. H. Jensen, S. Koseki, N. Matsunaga, K. A. Nguyen, S. Su, T. L. Windus, M. Dupuis, and J. A. Montgomery, Jr., *J. Comput. Chem.* **14**, 1347 (1993).
- ¹⁹C. M. Marian, R. Marian, S. D. Peyerimhoff, B. A. Hess, R. J. Buenker, and G. Seger, *Mol. Phys.* **46**, 779 (1982).
- ²⁰T. Ergler, A. Rudenko, B. Feuerstein, K. Zrost, C. D. Schröter, R. Moshhammer, and J. Ullrich, *Phys. Rev. Lett.* **95**, 093001 (2005).
- ²¹P. von den Hoff, I. Znakovskaya, S. Zherebtsov, M. F. Kling, and R. de Vivie-Riedle, *Appl. Phys. B* **98**, 659 (2010).
- ²²S. Petretti, Y. V. Vanne, A. Saenz, A. Castro, and P. Decleva, *Phys. Rev. Lett.* **104**, 223001 (2010).
- ²³S. Petretti, A. Magaña, A. Saenz, and P. Decleva, *Phys. Rev. A* **94**, 053411 (2016).
- ²⁴V. P. Majety and A. Scrinzi, *Phys. Rev. Lett.* **115**, 103002 (2015).
- ²⁵L. J. Frasinski, J. Plumridge, J. H. Posthumus, K. Codling, P. F. Taday, E. J. Divall, and A. J. Langley, *Phys. Rev. Lett.* **86**, 2541 (2001).
- ²⁶X. Sun, R. L. Fu, K. Yonemitsu, and K. Nasu, *Phys. Rev. Lett.* **84**, 2830 (2000).
- ²⁷A. O. Lindahl, J. Rohlén, H. Hultgren, I. Y. Kiyani, D. J. Pegg, C. W. Walter, and D. Hanstorp, *Phys. Rev. Lett.* **108**, 033004 (2012).